RESULTS AND DISCUSSION

1. Preparation and characterization of nickel aluminate precursor by the One Pot Synthesis.

As previously described, the One Pot Synthesis is the simplest chemical process that can produce oligomeric precursors containing any combination of metal oxides in one step.

Due to the advantages of this process over traditional methods, including the potential to control product homogeneity and purity, to lower processing temperatures and times, and to control the size, shape, and size distribution of the resulting ceramic particles.

In this work, metallo-organic precursor of $NiAl_2O_4$ was synthesized in a similar way as previously reported for synthesizing $MgAl_2O_4$ double alkoxide precursor. Four nickel(II) salts: nickel nitrate hexahydrate, nickel chloride hexahydrate, nickel hydroxide and nickel acetate tetrahydrate were employed to react with $Al(OH)_3.xH_2O$ and triethanolamine to study the possibility to prepare nickel-organic precursor.

According to the amount of hydrate water in commercial aluminium hydroxide hydrate is vary, depending on atmospheric moisture. $Al(OH)_3.xH_2O$ was calcined in TGA to determine percentage of Al_2O_3 before introduced as starting material for sample preparation. Additionally, the exact percentage of NiO resulting from calcination of the preparative $Ni(OH)_2$ which obtained from precipitation method between aqueous solution of 0.5 mol/l nickel chloride and concentrate ammonia [25%(w/w)], was investigated by TGA. Elimination of water molecules and decomposition of hydroxide from $Al(OH)_3.xH_2O$ and $Ni(OH)_2$ were confirmed by mass loss in the TGA, corresponding to the equations:

$$2Al(OH)_3.xH_2O \xrightarrow{\Delta} Al_2O_3 + (x+3)H_2O \quad ...(10)$$

$$Ni(OH)_2 \xrightarrow{\Delta} NiO + H_2O \quad ...(11)$$

The resulting TGA curves of $Al(OH)_3.xH_2O$ and $Ni(OH)_2$ as shown in Appendix A, Figure A1 and Figure A2 revealed the ceramic yields for Al_2O_3 and NiO to be 63.2 and 66.4%(w/w), respectively. Both values were used throughout these experiments.

The reaction mixture of $Al(OH)_3.xH_2O$, nickel(II) salt and TEA in ethylene glycol was completely after distillation for 6-8 h, resulting in a clear colored solution. With respect to the reaction in equation 12, four precursors, namely SPNO, SPCl, SPOH and SPAc occurred, corresponding to the nickel(II) salts; $Ni(NO_3)_2.6H_2O$, $NiCl_2.6H_2O$, $Ni(OH)_2$ and $Ni(CH_3COO)_2.4H_2O$, respectively (see Table 5).

$$2Al(OH)_3.xH_2O + \left\{ \begin{array}{c} Ni(NO_3)_2.6H_2O \\ NiCl_2.6H_2O \\ Ni(OH)_2 \\ Ni(CH_3COO)_2.4H_2O \end{array} \right\} + 3TEA + x' EG \xrightarrow[-H_2O]{140^{\circ}C \,/\, 7\ h} \text{Spinel Precursor} \quad ...(12)$$

To remove ethylene glycol solvent, further distillation was required until the viscous precursor was noticed. However, this must be done with care because the precursor is easy to burn. In standing at room temperature, the viscous precursors, except SPCl became solid. The color and physical appearances of nickel aluminate precursors were presented in the Table 5.

Table 5 The color and physical appearances of nickel aluminate precursors.

Ni(II) salt used for precursor preparation	Notation of precursor	Color of viscous precursor	Appearance of solid precursor
$Ni(NO_3)_2.6H_2O$	SPNO	Black	Hard and rigid solid
$NiCl_2.6H_2O$	SPCl	Light green	Clear viscous liquid
$Ni(OH)_2$	SPOH	Dark green	Brittle solid
$Ni(CH_3COO)_2.4H_2O$	SPAc	Bright green	Sticky solid

The black color of SPNO might be due to HNO_3 is formed in the solution during the reaction goes on. Basically, HNO_3 is the oxidizing acid, therefore organic compound in the solution such as TEA and EG can be oxidized. Consequently, the color of SPNO is different from other nickel precursors.

The solubility of precursors was tested. It was found that all precursors easily dissolved in water, dimethyl sulfoxide and alcohols, such as methanol, ethanol, n-propanol, iso-propanol but were not dissolved in acetonitrile and chloroform.

Due to the high boiling points of TEA (335.4°C) and EG (198°C), it is difficult to remove excess TEA and EG. The excess TEA and EG were thus retained in the precursors which cause the interferences in nickel aluminate precursors characterization. However, excess TEA and EG can be burned out during the pyrolysis of the precursors.

To avoid the contamination of EG and TEA, attempted to purify precursors was performed. Acetonitrile was slowly added to the precursor which was readily dissolved in methanol with constant stirring. The precipitate were collected by suction filtration and washed with deionized water before drying at 110°C for 2 h in an oven, resulting black SPNO and green SPCl. Unfortunately, precipitation of SPOH and SPAc precursors failed

in any solvents. Although there are only two dried solid precursors; SPNO and SPCl, characterization of these solids and crude (SPOH and SPAc) precursors were carried out.

The structural information of all precursors obtained was determined by using electro spray ionization (ESI) techniques. The major peak as the protonated parent ion was appeared at m/z = 554 for both solid SPNO and SPCl including crude SPAc (see Appendix B, Figure B1, B2 and B4), except SPOH precursor which showed the mass fragmentation at *m/z* = 528 (see Appendix B, Figure B3). The possible structure of precursors was proposed to be a trimetallic species, consisting of one TEA ligand per metal center. To minimize the charge separation for the most stable structure for the dipositive cation precursor, therefore, it was assumed that Ni^{2+} ion was enfolded by the third TEA (Figure 10).

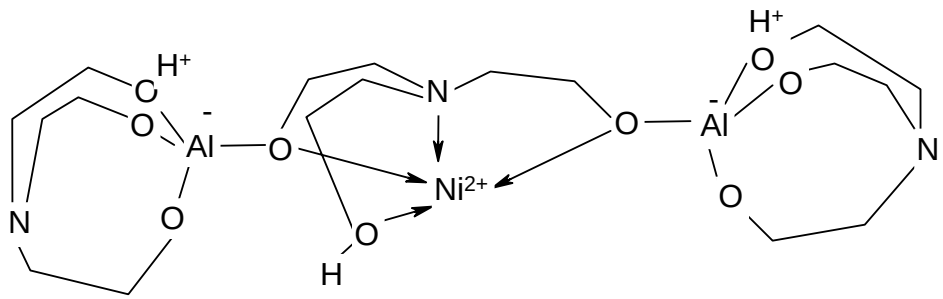

Figure 10 Nickel aluminate precursors (m/z =554)

In the case of crude SPOH precursor, the possible structure of crude SPOH fragment with *m/z* = 528 was proposed to be a degradation trimetallic species of the nickel aluminate spinel precursor. The $-CH_2CH_2OH$ of bridging TEA group may be decomposed and the occurring -OH group probably coordinates to the Ni^{2+} cation as shown in Figure 11.

The proposed nickel aluminate precursor's structure (Figure 10) is similar to that of magnesium aluminate precursor which prepared in the same manner as presented in

equation 1 (section spinel preparation). The difference is only the central unit in which Ni^{2+} ion is coordinated to triethanolamine for the former precursor, where in the latter is Mg^{2+} ion.

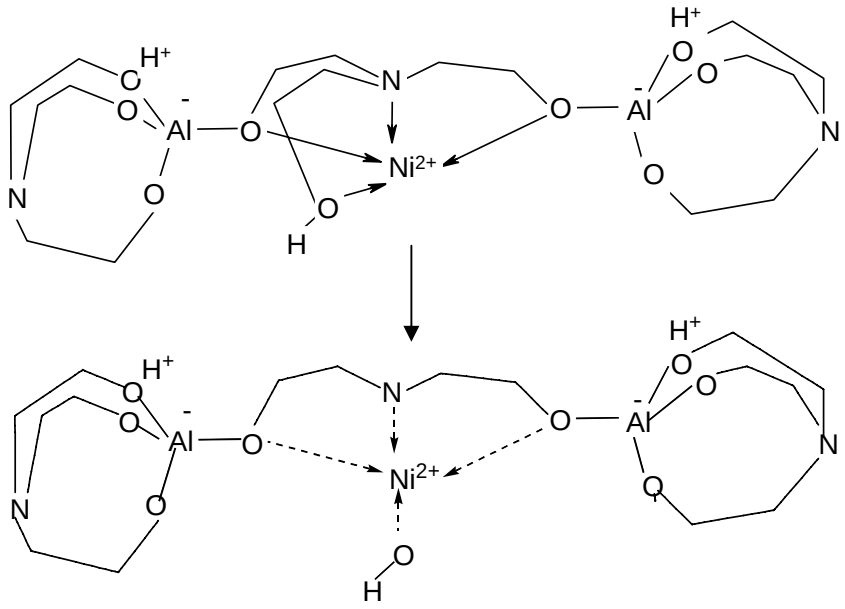

Figure 11 The degradation of the nickel aluminate spinel precursor

^{1}H-NMR results for nickel aluminate precursors are presented in Appendix C, Figure C1 – Figure C4 and summarized in Table 6.

Table 6 ^{1}H-NMR peak positions and assignments of nickel aluminate spinel precursors

Tentative assignment	Peak position (ppm)			
	Solid SPNO	Solid SPCl	Crude SPOH	Crude SPAc
$N(C\boldsymbol{H_2}CH_2OH)_3$, free TEA	-	-	2.33 (t)	2.55 (t)
$N(CH_2C\boldsymbol{H_2}OH)_3$, free TEA	-	-	3.35 (t)	3.38 (t)
$NC\boldsymbol{H_2}CH_2OAl$	2.49 (t)	2.49 (t)	2.50 (t)	2.63 (t)
$NCH_2C\boldsymbol{H_2}OAl$	3.33 (t)	3.33 (t)	3.42 (t)	3.47 (t)
OH of TEA either coordinated to Ni^{2+} or free TEA	4.45 (br)	4.45 (br)	4.48 (br)	4.44 (br)

^{1}H-NMR peak positions of solid SPNO and SPCl appeared exactly at the same positions, for methylene groups adjacent to oxygen and nitrogen atoms, occurring at chemical shifts of 3.33 ppm (triplet) and 2.49 ppm (triplet), respectively. This variability is due to the fact that the protons in methylene groups are surrounded by electrons and exist in slightly different electronic environments from one another. Both peak positions shift around 0.2 ppm downfield position as comparing between metal-TEA complexation and free TEA.

^{1}H-NMR spectrum of crude SPOH and SPAc showed peak positions of precursor methylene groups adjacent to oxygen and nitrogen atoms at chemical shifts around 3.42 – 3.47 ppm (triplet) and 2.50 – 2.63 ppm (triplet), respectively. Moreover, ^{1}H-NMR spectra revealed peak positions of free TEA methylene groups around 3.35 – 3.38 ppm (triplet) and 2.33 – 2.55 ppm (triplet). These peaks indicated that the excess TEA still retained in the precursors because of its high boiling point, hence, it was difficult to remove from the reaction. This result is similar to that of Waldner work (Waldner *et al*., 1996). Noticeably, peak positions of crude SPOH and SPAc methylene groups are

slightly shift from solid SPNO and SPCl. Because the remained TEA in crude SPOH and SPAc probably interrupt the induce magnetic field of the major specie in the precursor.

^{13}C-NMR results for nickel aluminate precursors are shown in Appendix C, Figure C5 – Figure C8 and summarized in Table 7.

Table 7 ^{13}C-NMR peak positions and assignments of nickel aluminate spinel precursors

Tentative assignment	Peak position (ppm)			
	Solid SPNO	Solid SPCl	Crude SPOH	Crude SPAc
$N(\mathbf{C}H_2CH_2OH)_3$, free TEA	-	-	57.16	54.15
$N(CH_2\mathbf{C}H_2OH)_3$, free TEA	-	-	59.36	59.34
$N\mathbf{C}H_2CH_2OAl$	54.76	54.76	57.21	57.10
$NCH_2\mathbf{C}H_2OAl$	60.91	60.91	62.87	60.24
Bridging $N\mathbf{C}H_2CH_2O$	59.87	59.87	59.29	58.91
Bridging $NCH_2\mathbf{C}H_2O$	63.45	63.45	69.05	62.78

Similar to the ^{1}H-NMR results, the ^{13}C-NMR spectra of solid SPNO and SPCl were identical in chemical shifts which consist of four different peaks related to the carbon positions in the structural precursors. The peaks at chemical shifts of 54.76 and 60.91 ppm are assigned to the carbon of ethyleneoxy groups bound to Al while the peaks at chemical shifts of 59.87 and 63.45 ppm are the most probably positions for the bridging TEA ligand. ^{13}C-NMR spectrum of crude SPOH and SPAc exhibited peak positions of ethyleneoxy groups carbon bound to Al at chemical shifts around 57.10 – 57.21 ppm and 60.24 – 62.87 ppm, while the peaks at chemical shifts around 58.91 – 59.29 ppm and 62.78 – 69.05 ppm are the most likely positions for the bridging TEA ligand. Furthermore, ^{13}C-NMR spectra demonstrated peak positions of free TEA ethyleneoxy group's carbon around 54.15 – 57.16 ppm and 59.34 – 59.36 ppm, in agreement with

the discovering of excess TEA from ^{1}H-NMR results. However, the retained of free TEA can be burned out during the pyrolysis. The existance of free TEA in the precursor could be confirmed by a decreasing of ceramic yield in TGA analysis. Comparison ^{13}C-NMR spectra of crude SPOH and SPAc to those solid SPNO and SPCl, it was found that all corresponding peak positions are slightly different with chemical shift around 0.50 - 5.60 ppm. The discussions of ^{13}C-NMR results are similar to that of ^{1}H-NMR results.

The Distortionless Enhancement by Polarization Transfer (DEPT) results of the precursor consist of negative (inverse) peaks (see Appendix C, Figure C9 – Figure C12). All of negative peaks in the spectrum showed that carbon in the nickel aluminate spinel precursor are methylene groups (-CH_2).

According to the previous results, it is indicated that the ^{13}C-NMR and DEPT support ^{1}H-NMR results. This confirms that the structure of precursor proposed is reasonable.

Decomposition of organic content in precursor samples was followed by TGA analysis. TGA thermogram of dried solid; SPNO and SPCl are slightly different as shown in Appendix A, Figure A3 and Figure A4; respectively. Thermograms show three regions of mass loss. The first mass loss occurring between 50°C and 300°C was involved the decomposition of the organic content. In this step, volatiles and char were generated (Waldner *et al*., 1996). The char obtained was then oxidizes during continuous heating from 300°C to 400°C as shown in the region of second mass loss. The final mass loss occurred at 400°C and 800°C. It should be noted that in the final mass loss, few of $NiCO_3$ is formed. The formation of $NiCO_3$ during ligand decomposition could be confirmed by the FTIR result which shows the low intensity and broad peak at 1508 cm^{-1} and 1413 cm^{-1} (see Appendix D, Figure D3, c).

Thermal decomposition profiles of solid SPNO and SPCl were similar as compared to that of crude SPOH and SPAc (see Appendix A, Figure A5 and Figure A6). However, crude precursors revealed higher weight loss, indicating the excess of TEA and EG retained in crude precursors. Table 8 illustrated percentage weight loss and ceramic yields of all analyzed precursors.

Reference to the proposed structure of nickel aluminate precursor (Figure 10), assuming all organic content are decomposed on heat treatment and generated the nickel aluminate spinel, $NiAl_2O_4$ as the final product which could be analyzed by X-ray diffraction. The calculated theoretical weight loss and ceramic yield are found to be 68.10 and 31.90 %(w/w), respectively (see Appendix A).

The experimental weight loss of solid SPNO [68.66 %(w/w)] and SPCl [70.59 %(w/w)] are consistent with the calculated theoretical weight loss of 68.10 %(w/w). The percentage ceramic yields of the solid SPNO [31.34 %(w/w)] and SPCl [29.41 %(w/w)] were in excellent agreement with the theoretical value [31.90 %(w/w)], the results indicated that the excess TEA and EG were not retained in the solid precursors. On the other hand, the higher relative weight loss of crude SPOH [85.94 %(w/w)] and SPAc [80.91 %(w/w)] as compared to that of solid precursors (see Table 8), confirms that there are extra TEA and EG contaminated in crude precursors, resulting in lower relative ceramic yields of 14.06 and 19.09 %(w/w) for crude SPOH and SPAc, respectively. This is around 12.80 – 17.80 %(w/w) differ from theoretical value.

Table 8 Percentage weight loss and ceramic yield of the nickel aluminate precursors

Nickel precursor	Weight loss (%w/w)	Ceramic yield (%w/w)
Solid SPNO	68.66	31.34
Solid SPCl	70.59	29.41
Crude SPOH	85.94	14.06
Crude SPAc	80.91	19.09

The valuable information obtained from NMR and TGA analyse suggested a high purity of solid precursor. Therefore, Fourier Transform Infrared spectra of solid SPNO and SPCl are recorded. The results are represented in Appendix D, Figure D1 and Figure D2. Peak assignments are summarized in Table 9.

FTIR data are correlated to structural characteristics of precursor proposed shown in Figure 10, the broad peaks at 3420 and 3410 cm^{-1} are characteristic of H-bonded, O-H stretching. The peak positions at 1628 and 1636 cm^{-1} are assigned to O-H bending of OH group. The peak positions at 3000, 1383 – 1433 and 725 cm^{-1} are corresponded to C-H stretching, C-H bending and -CH_2 rocking (Cooper, 1980) of methylene groups, respectively. Despite a similarity of FTIR spectra, it was observed that the O-H bending (1628 cm^{-1}) and C-H bending intensity (1383 cm^{-1}) for SPNO are relatively high as compared to that of SPCl (see Appendix D, Figure D2). It might be due to an overlapping of O-H and C-H bending with asymmetric and symmetric stretching frequencies of trace NO_3^- from starting material [$Ni(NO_3)_2.6H_2O$] which occurred in the range of 1650 – 1600 cm^{-1} and 1400 – 1350 cm^{-1}, respectively (Conley, 1966). The metal and TEA coordinating atom showed a broad peak of Al-O-C at 1072 - 1075 cm^{-1}. The peaks at 657 - 661 cm^{-1} are assigned to metal oxygen bridging, Al-O-Ni bond (Thanabodeekij *et al,* 2003).

Table 9 FTIR peak positions and assignments of nickel aluminate spinel precursors

Nickel precursor	Peak assignment (cm^{-1})						
	O-H(ν)	O-H(δ)	C-H(ν)	C-H(δ)	$-CH_2$(ρ)	Al-O-C(ν)	Al-O-Ni(ν)
Solid SPNO	3420	1628	3000	1383	725	1072	657
Solid SPCl	3410	1636	3000	1433	725	1075	661

2. Preparation and characterization of nickel aluminate spinel

2.1 Preparation and characterization of nickel aluminate spinel directly from nickel aluminate precursor.

Calcination of crude organic precursors (SPNO, SPCl, SPOH and SPAc) with the temperature ranging from 500°C to 1000°C for 5 h produced grayish-green, green or blue solid products, depending on the temperature applied.

Fourier Transform Infrared Spectroscopy of the color products obtained was initially studied in order to follow precursor decomposition and spinel evolution at the atomic level. The infrared spectra of the products obtained from the crude SPNO, SPCl, SPOH and SPAc are similar and shown identical in wave number as illustrated in Appendix D, Figure D3 – D6. All calcined products showed a broad peak at 3436 cm^{-1}, attributable to *v*(OH) of physisorbed water or hydrogen-bonded hydroxyl groups on the surface. However, calcination temperature below 800°C illustrated the formation of $NiCO_3$ during ligand decomposition which is indicated by broad peaks at 1508 and 1413 cm^{-1} (Appendix D, Figure D3 (a) – (c) – Figure D6 (a) – (c)), identified by comparison with published literature (Waldner *et al.*, 1996). With increasing calcination temperature up to 800, 900 and 1000°C, the carbonate peaks are no longer discernible (Appendix D, Figure D3 (d) – (f) – Figure D6 (d) – (f)) as the carbonate decomposition, losing CO_2. Additionally, two characteristic peaks of the nickel aluminate, $NiAl_2O_4$ spinel phase at 727 and 500 cm^{-1} appear which associated with the lattice vibrations of tetrahedrally coordinated Al-O (Grimes, 1994) and stretching vibration mode of Al-O for the octahedrally coordinated aluminium ion, respectively (Preudhomme and Tarte, 1971 or Allen and Paul, 1995). Further characterization by X-ray diffraction to confirm $NiAl_2O_4$ spinel phase was performed.

The effect of temperature and the range of heating time on the formation of $NiAl_2O_4$ phase from pyrolysis of the spinel precursor were investigated by X-ray diffraction technique. X-ray diffraction patterns of calcined products at various temperatures ranging from 500°C to 1000°C with a fixed 5 h heating period were shown in Appendix E, Figure E2 – Figure E5 and summarized in Table 10. The X-ray diffraction results of SPNO, SPCl and SPAc precursors calcined at 500, 600 and 700°C clearly showed NiO phase indicating by the major peaks at 111 *hkl* reflection (d = 0.241 nm, *I* = 61.0 %), 200 *hkl* reflection (d = 0.209 nm, *I* = 100.0 %) and 220 *hkl* reflection (d = 0.148 nm, *I* = 35.0 %) (see Appendix E, Figure E2, (a) – (c), Figure E3, (a) – (c), and Figure E5, (a) – (c)), corresponding to the JCPDS file No. 44 – 1159. The X-ray diffraction pattern of the SPOH precursor calcined at 500°C and 600°C as illustrated in Appendix E, Figure E4 (a) – (b) revealed mixed phases of Ni and NiO. The Ni phase was evidenced by the major peaks at 111 *hkl* reflection (d = 0.203 nm, *I* = 100.0 %) and 200 *hkl* reflection (d = 0.176 nm, *I* = 42.0 %) (see Appendix E, Figure E4, (a) – (b)), as compared to the JCPDF file No 04 - 0850. At 800°C, the peaks of $NiAl_2O_4$ spinel phase with 400 and 440 *hkl* reflections at 2θ 45.00 and 65.54, respectively were observed with the addition of NiO (see Appendix E, Figure E2(d), Figure E3(d), Figure E4(d) and Figure E5(d)). The major peak for $NiAl_2O_4$ spinel with 311 *hkl* reflection at 2θ 37.01 is obviously seen and appeared as a broad peak because of the overlap with the NiO (111 *hkl* reflection) peak. Detection of $NiAl_2O_4$ phase at 800°C by X-ray diffraction is consistent with the FTIR spectra result which illustrated the characteristic for the $NiAl_2O_4$ structure absorption bands at 727 and 500 cm^{-1} (see Appendix D, Figure D3(f)). With increasing temperature to 900°C, it should be noted that the NiO phase still remained in the product containing $NiAl_2O_4$ (see Appendix E, Figure E2(e), Figure E3(e), Figure E4(e) and Figure E5(e)). It was found that the intensity of *hkl* reflections for NiO phase gradually decrease with increasing temperature (see Appendix E, Figure E2 (a) – (e) – Figure E5 (a) – (e)). This illustrated that $NiAl_2O_4$ phase was enhanced as the increasing calcination temperature from 800 to 900°C. At 1000°C, single phase of $NiAl_2O_4$ spinel was formed when SPNO and SPAc were calcined, evidenced by the major peaks at 311

hkl reflection (d = 0.242 nm, *I* = 100.0 %), 400 *hkl* reflection (d = 0.201 nm, *I* = 65.0 %) and 440 *hkl* reflection (d = 0.142 nm, *I* = 60.0 %) (see Appendix E, Figure E2(f) and Figure E5(f)), in good agreement to the JCPDS file No. 10-0339 (see Appendix E, Figure E1). However, after calcinations of SPCl and SPOH at 900°C or even at 1000°C, X-ray diffraction patterns showed two crystalline phases, NiO and $NiAl_2O_4$ (see Appendix E, Figure E3 (e) – (f) – Figure E4 (e) – (f)). It suggested that increasing of calcination temperature above 1000°C necessary to enhance a single $NiAl_2O_4$ phase. All calcined products detected $NiAl_2O_4$ phase by X-ray diffraction are in agreement with the FTIR results (see Appendix D, Figure D3 – Figure D6).

Table 10 X-ray diffraction analysis of product phases calcined at different temperature with a fixed 5 h heating period

Calcination Temperature (°C)	Calcined product phase			
	SPNO	SPCl	SPOH	SPAc
500	NiO	NiO	NiO+Ni	NiO
600	NiO	NiO	NiO+Ni	NiO
700	NiO	NiO	NiO	NiO
800	NiO+$NiAl_2O_4$	NiO+$NiAl_2O_4$	NiO+$NiAl_2O_4$	NiO+$NiAl_2O_4$
900	NiO+$NiAl_2O_4$	NiO+$NiAl_2O_4$	NiO+$NiAl_2O_4$	NiO+$NiAl_2O_4$
1000	$NiAl_2O_4$	NiO+$NiAl_2O_4$	NiO+$NiAl_2O_4$	$NiAl_2O_4$

Effect of soaking time on the formation of spinel phase was also studied. The XRD patterns of resulting product obtained by calcinations of SPNO, SPCl, SPOH and SPAc at 1000°C for different soaking periods of 2, 3, 4 or 5 h were analyzed and summarized in Table 11. Two phases, $NiAl_2O_4$ and NiO, are detected for calcined samples with soaking time of 2, 3 and 4 h (see Appendix E, Figure E6, (a) – (c) – Figure E9, (a) – (c)). Calcination of SPCl and SPOH at 1000°C along with 5 h calcination time or even longer, the NiO phase still remained in product containing $NiAl_2O_4$. However, the

$NiAl_2O_4$ spinel completely formed only calcination products of SPNO and SPAc with heating for 5 h at 1000°C (see Appendix E, Figure E6 (d) and Figure E9 (d)). Due to the prolonging of calcination time enhance $NiAl_2O_4$ yield. Hence, the NiO could be completely removed by increasing the calcination time.

Table 11 X-ray diffraction analysis of product phases calcined at different heating period with a fixed 1000°C calcination temperature

Heating period (h)	Calcined product phase			
	SPNO	SPCl	SPOH	SPAc
2	$NiO+NiAl_2O_4$	$NiO+NiAl_2O_4$	$NiO+NiAl_2O_4$	$NiO+NiAl_2O_4$
3	$NiO+NiAl_2O_4$	$NiO+NiAl_2O_4$	$NiO+NiAl_2O_4$	$NiO+NiAl_2O_4$
4	$NiO+NiAl_2O_4$	$NiO+NiAl_2O_4$	$NiO+NiAl_2O_4$	$NiO+NiAl_2O_4$
5	$NiAl_2O_4$	$NiO+NiAl_2O_4$	$NiO+NiAl_2O_4$	$NiAl_2O_4$

The powder diffraction patterns of calcined products obtained by calcination at 1000°C for 5 h and step calcination (500°C for 5 h and held at 1000°C for 5 h) are compared as illustrated in Appendix E, Figure E10 – Figure E13. For both condition, the diffraction peaks of SPNO and SPAc pyrolyzed products indicate the phase purity of the $NiAl_2O_4$ spinel (see Appendix E, Figure E10 and Figure E13). In contrast, the XRD patterns of SPCl and SPOH pyrolyzed products exhibit NiO phase with the addition of $NiAl_2O_4$ spinel (see Appendix E, Figure E11 and Figure E12).

The SEM micrographs of the spinel powder prepared from SPNO, SPCl, SPOH and SPAc precursors are shown in Appendix F, Figure F1 – Figure F4. All $NiAl_2O_4$ powders showed a porous microstructure with irregular shaped of block-like particles. However, the formation of several agglomerates was detected. The porous may have been formed during the decomposition of organic ligand and volatile hydrocarbon as the precursors were heated. Additionally, after pyrolysing the precursor, occurring of

CO_3^{2-} which confirmed by TGA and FTIR could be decomposed to CO_2. All of which are difficult to escape from a high-viscous precursor, consequently, gas-filled, foam-like and pore between grain boundaries structure is obtained (Laobuthee *et al*., 2000). The $NiAl_2O_4$ powder prepared from SPNO, SPOH and SPAc precursors showed a similar morphology with nonuniform particles due to the effect of the agglomeration (see Appendix F, Figure F1 (a) – (b), Figure 2, (a) – (b) and Figure 4, (a) – (b)), while in the case of SPCl more uniform, block-like particles was obtained (see Appendix F, Figure 3, (a) – (b)).

The SEM observations of the $NiAl_2O_4$ powder obtained from non step (1000°C, 5 h) and step calcination (500°C, 5h and 1000°C, 5 h) showed a similar morphology as confirmed by surface area and porosity characteristics of the powders illustrated in Table 12. By comparing the specific surface area, pore volume and pore size of $NiAl_2O_4$ spinel at both calcined conditions; it shows that these values are not significantly different. The results from BET and SEM indicate that the $NiAl_2O_4$ powder obtained has not high surface area, however the largest specific surface area of $NiAl_2O_4$ obtained from SPCl ($\approx$ 46 m^2/g) was due to its homogeneous particles distribution as seen in Appendix F, Figure F3, (a) – (b). The $NiAl_2O_4$ spinels from One Pot Synthesis process are a highly pure compound as comparing with other previous work (Han *et al*., 2004).

Table 12 The BET surface areas, pore volume and pore size of $NiAl_2O_4$ spinels which directly obtained from nickel aluminate precursor

Nickel precursor	Heat treatment	BET surface area (m^2/g)	Pore volume (cm^3/g)	Pore size (nm)
SPNO	1000 °C (5 h)	31.99	0.09	12.28
	500 (5 h) and 1000 °C (5 h)	31.08	0.10	13.14
SPCl	1000 °C (5 h)	46.92	0.13	11.27
	500 (5 h) and 1000 °C (5 h)	46.34	0.14	12.12
SPOH	1000 °C (5 h)	39.23	0.08	8.40
	500 (5 h) and 1000 °C (5 h)	39.66	0.09	9.21
SPAc	1000 °C (5 h)	22.58	0.04	8.97
	500 (5 h) and 1000 °C (5 h)	22.33	0.05	9.81